JOURNAL OF SPACECRAFT AND ROCKETS
Vol. 44, No. 3, May–June 2007

Simplified Computational Models for Shear-Compliant Borders in Solar Sails

Jack Leifer*
Trinity University, San Antonio, Texas 78212

DOI: 10.2514/1.20907

Shear-compliant regions have been demonstrated to reduce both the amplitude and extent of structural wrinkles on the surface of thin-film (gossamer) membranes under simultaneous tension and shear. Rather than modeling the full geometric details of the thermoformed strips that comprise a shear-compliant region, two simplified approaches have been developed for efficiently incorporating them into existing finite element models. One approach replaces the three-dimensional geometry of the thermoformed region with alternating flat strips of high-stiffness/Poisson's ratio and low-stiffness/near-zero Poisson's ratio materials. The other approach uses a properly aligned uniaxial orthotropic material to model the behavior of the shear-compliant region. Both approaches were simulated in finite element software and yielded similar results that qualitatively reflected the behavior of existing membrane test articles containing thermoformed shear-compliant regions. However, numerical results obtained using the model containing the orthotropic material were highly sensitive to the ratio of Young's moduli used to compute the values of the orthotropic material parameters.

Nomenclature

E_f, E_m	=	Young's moduli of the low- and high-compliance components of the orthotropic shear-compliant region
E_{high}, E_{low}	=	general representation for high and low values of Young's moduli used in the various numerical models tested
E_{nominal}	=	Young's modulus of the unthermoformed membrane materials
$E_{\text{thermoformed}}$	=	Young's modulus within the thermoformed strips
G_f, G_m	=	shear moduli of the low- and high-compliance components of the orthotropic shear-compliant region
K_f, K_m	=	lateral compression moduli (without longitudinal deformation) of the low- and high-compliance components of the orthotropic shear-compliant region
k_f, k_m	=	bulk moduli of the low- and high-compliance components of the orthotropic shear-compliant region
L, T, T'	=	longitudinal, transverse, and out-of-plane coordinate directions
V_f, V_m	=	volume fraction parameters of the low- and high-compliance components of the orthotropic shear-compliant region
x	=	longitudinal direction
y	=	transverse direction
z	=	out-of-plane direction
ν_f, ν_m	=	Poisson's ratio of the low- and high-compliance components of the shear-compliant region
σ_2	=	second principal stress

Presented as Paper 2056 at the 46th AIAA/ASME/ASCE/AHS/ASC Structures, Structural Dynamics & Materials Conference, Austin, TX, 18–21 April 2005; received 6 November 2005; revision received 4 August 2006; accepted for publication 18 December 2006.

*Assistant Professor, Department of Engineering Science, One Trinity Place. Member AIAA.

I. Introduction

WORK is continuing at NASA toward the goal of advancing solar sail systems to a Technology Readiness Level (TRL) of 6, which requires testing and validation of scale-model prototypes in relevant environments [1]. Many of the proposed designs for solar sails envision a square geometry of up to 100 m per side, comprising triangular quadrants fabricated from thin-film material (Fig. 1) and attached to lightweight booms at their corners.

Sails of this type are currently being designed under the aegis of the NASA In-Space Propulsion Program. One difficulty associated with the tensioned membranes that comprise the sail is the formation of reversible structural (elastic) surface wrinkles. These wrinkles occur when the membrane is not maintained in a state of biaxial tension. Structural wrinkles can arise from thermal strains caused by temperature gradients over the extent of the membrane area or supports, or from small misalignments, inhomogeneities, or strains introduced by the support structure. Regardless of their cause, wrinkles are caused by a localized buckling within the membrane and are generally located in regions in which σ_2 becomes slightly compressive [2]. The amplitude and extent of structural wrinkling of the membrane surface can be reduced by the use of an integrated shear-compliant border, such as that described by Talley et. al [3] (Figs. 2 and 3). This particular shear-compliant geometry consists of thin, thermoformed, parallel ridges integrated into the face of an otherwise flat membrane. The longitudinal axis of each ridge is initially perpendicular to the nearest adjacent membrane edge. Such shear-compliant borders are designed to maintain the membrane surface in a state of biaxial tension by absorbing the bulk of the extraneous strains, therefore reducing the formation of structural wrinkles across the membrane surface. Although it has been demonstrated experimentally that shear-compliant borders can effectively maintain a state of biaxial tension over the entire surface of a membrane, computational tools for optimizing border geometry for a particular membrane have not been developed [4]. This is due in part to the excessively large models required to numerically simulate the geometry of shear-compliant borders in fine detail. Hence, alternative strategies incorporating simpler (yet functionally equivalent) numerical models of the shear-compliant region are sought. This work compares two possible schemes for simplified finite element (FE) models of membranes containing shear-compliant borders.

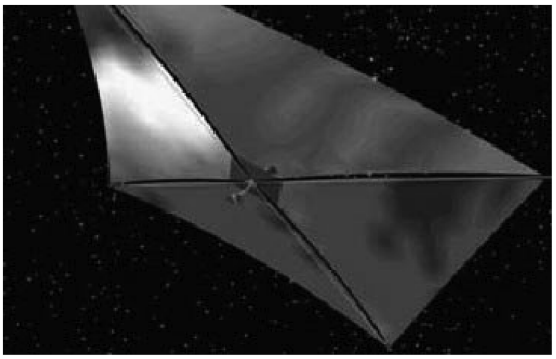

Fig. 1 Square solar sail concept consisting of four triangular quadrants supported by booms (from Gaspar et al. [14]).

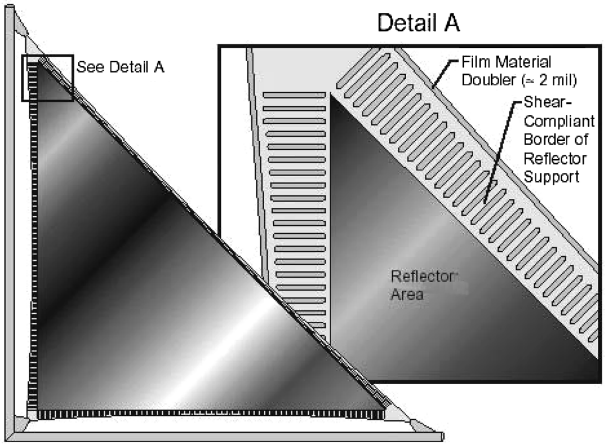

Fig. 2 Placement of shear-compliant borders around the perimeter of a triangular sail quadrant (from Talley et al. [3]).

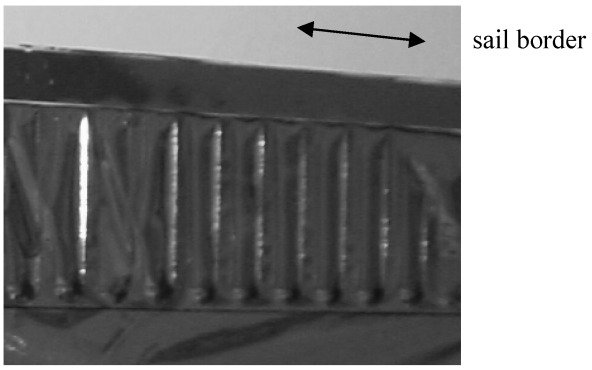

Fig. 3 Photograph of thermoformed elements along the perimeter of a triangular sail quadrant.

II. Prior Work

The effect of surface structural wrinkling on the performance of solar sails has been the subject of much recent debate. Though it is now generally believed that the presence of wrinkles will not have a deleterious effect on the net thrust imparted to a solar sail [5], they may have other consequences that affect sail performance. Chief among these is the concern that deep wrinkles could cause incident light to reflect from side to side within a single wrinkle, generating one or more localized "hot spots" on the sail surface. Such hot spots could lead to uneven thermal expansion of the sail surface, or even, in extreme cases, localized melting [5]. To reduce such problems, the use of an integrated shear-compliant border to minimize the formation of wrinkles has been incorporated into many of the sail designs currently under evaluation. Although it is known that the geometry of the shear-compliant border will determine its effectiveness in resisting the formation of surface wrinkles, no general guidelines for their design currently exist in the literature [4,6]. An efficient strategy for incorporating shear-compliant borders into existing finite element models is a first step toward optimizing their geometry for maximum effectiveness.

A detailed finite element model of a membrane containing thermoformed shear-compliant strips was tested by Leifer and Belvin [6]. The test article modeled in that particular simulation contained a central shear-compliant region thermoformed into a 0.140×0.178 m membrane. Figure 4 is a photograph of one such membrane, along with a membrane of similar size that does not contain the thermoformed features. Both of these polyester membranes are shown undergoing an applied transverse edge displacement. It is apparent in the photograph on the right that the thermoformed strips effectively prevent the formation of wrinkles in the margin areas (adjacent to the top and bottom edges) under the applied displacement [3]. The computational model of this particular test article, implemented in ANSYS 5.6 finite element software using about 100,000 SHELL 64 elements, incorporated the shear-compliant region by constructing a detailed three-dimensional geometric representation of each thermoformed strip (Fig. 5). Simulations performed with the finite element model predicted the same flat, wrinkle-free margins under the edge displacement that is apparent in the test article containing the thermoformed strips [6]; however, the large number of elements required to precisely represent the shape of each thermoformed strip renders this approach ill-suited for modeling large membranes (some of which could encompass areas exceeding thousands of square meters) incorporating shear-compliant regions. Convergence difficulties prevented testing the numerical response of this membrane model at edge displacements greater than 0.2 mm [6].

III. New Simulation Approaches

As an alternative to creating a geometrically accurate representation of each thermoformed strip, a simplified approach to modeling the behavior of the shear-compliant region was pursued, based in part on previous works by Greschik and Mikulas [7] and

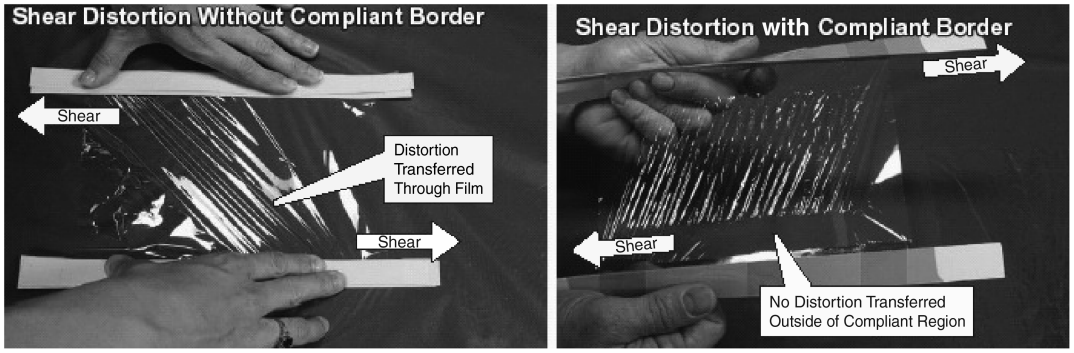

Fig. 4 The thermoformed shear-compliant region, shown in the membrane photographed on the right, maintains the top and bottom margins of the membrane wrinkle-free when it is displaced along its edges in the transverse (y) direction (from Talley et al. [3]). The dimensions of the membranes shown in the photographs are approximately 0.140×0.178 m.

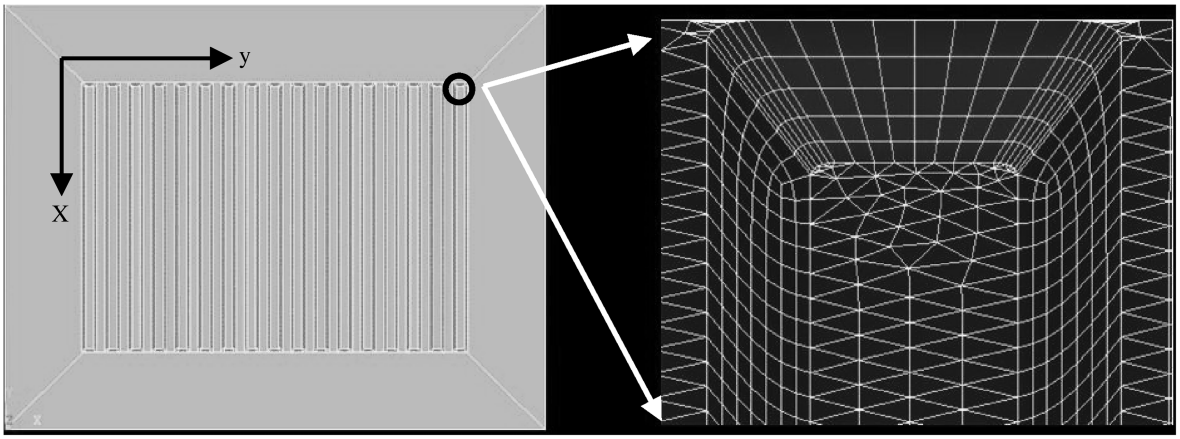

Fig. 5 The finite element model of the 0.140 × 0.178 m membrane test article shown in the right photograph of Fig. 4 includes geometric details of each thermoformed strip present in the central shear-compliant region. The fine mesh size required to adequately represent each thermoformed strip is illustrated by the close view of the FE mesh shown on the right (from Leifer and Belvin [6]).

Murphey [8,9], who analyzed membranes that contain material (permanent) wrinkles. Material wrinkles are typically caused by plastic (inelastic) deformation of the membrane created during the handling, folding, and transportation of thin films, and, unlike elastic wrinkles, do not disappear upon the removal of the applied external forces. Although the shear-compliant region under consideration was caused by a deliberate thermoforming process (rather than by deforming the bulk membrane material beyond its elastic limit), the strips formed by the thermoforming process strongly resemble long, thin material wrinkles. Similar to material wrinkles, thermoformed strips remain in the membrane after their initial formation, even in the absence of all external forces. The major difference between material wrinkles and the thermoformed strips is their width, because material wrinkles are much sharper (smaller radius of curvature) than the thermoformed strips.

Consider a long, thin material wrinkle (or thermoformed strip) with its y axis oriented across the wrinkle (transverse direction) and the x axis oriented along the wrinkle (longitudinal direction). According to Greschik and Mikulas [7], a tensile force directed across the wrinkle in the y direction will cause it to act like a hinge, with pure bending about the x axis. This bending occurs with negligible extensional surface strain in either the y or x directions. A tensile force applied in the longitudinal direction (x, along the axis of the wrinkle), however, causes the material to behave in accordance with Hooke's law. It is proposed that despite the difference in radius of curvature, the thermoformed strips demonstrate a hingelike behavior similar to that of the thin material wrinkles analyzed by Greschik and Mikulas. Hence, a first-order representation for the behavior of a membrane containing long, thin thermoformed strips must allow for high compliance when stressed in the transverse direction (i.e., E several orders of magnitude smaller than that provided by surface deformation), with little corresponding longitudinal strain (i.e., ν close to zero).

To estimate the equivalent Young's modulus of a material containing a single crease (material wrinkle) under an applied transverse stress, Greschik and Mikulas [7] performed experiments using 25.4-mm-wide strips of 76.2-μm-thick pure annealed aluminum foil. Uniaxial stress was applied to each sample across the wrinkle, along the length of the strip. The stress-strain behavior exhibited by each sample was plotted, and the resulting curve possessed two linear regions of different slopes. At high stresses, the effect of the wrinkle was nearly negligible, because the tensile force applied in this region was larger than that required to flatten the material. Hence, strain accrued through material surface deformation, and the measured Young's modulus within the high-stress-response region was equivalent to that expected for virgin (uncreased) material. At low-stress levels, however, strain was developed primarily due to bending within the crease, and the measured Young's modulus value within the low-stress response region was approximately three orders of magnitude lower than that obtained for high stresses. Based on these experimental results, the value of Young's modulus $E_{\text{thermoformed}}$ in the transverse direction (across the thermoformed strip) used in the simulation was initially approximated as three orders of magnitude lower than that of the bulk material E_{nominal}.

A numerical model that used this particular approach was implemented in ANSYS 8.1, by replacing each three-dimensional representation of a thermoformed strip (such as those shown in Fig. 5) with a flat strip that could be meshed by fewer elements and that required a far simpler solid model to implement. The isotropic material properties of each high-compliance strip were determined on the basis of the previous discussion (Young's modulus $E_{\text{thermoformed}}$ reduced by about three orders of magnitude from that of the bulk membrane material E_{nominal}; Poisson Ratio $\nu_{\text{thermoformed}}$ set to near zero), and the thickness of each strip was set equal to that of the bulk membrane material. Substitution of the flat strips for the three-dimensional thermoformed strips in the finite element model resulted in a simpler shear-compliant region that was nonetheless predicted to respond like a model containing a full three-dimensional representation of the shear-compliant region. Despite the comparative simplicity of the flat design versus the geometrically complex three-dimensional design of each shear-compliant strip, this particular approach still required the creation and meshing of one distinct flat strip in the finite element model for every thermoformed strip present in the shear-compliant region of the physical membrane.

A further geometrical simplification of the finite element model was obtained by replacing the flat strips in the shear-compliant region with one single homogenous material governed by a single set of orthotropic parameters. The orthotropic material properties were obtained by modeling the shear-compliant region as a uniaxial composite material composed of many high-compliance thermoformed strips (low E, $\nu \sim 0$) uniformly interspersed with strips of the unthermoformed membrane material (high E, $\nu \sim 0.33$). This approach is similar to that used for modeling the properties of flat composite materials consisting of uniaxial strands or fibers impregnated with an adhesive matrix. Here, the thermoformed material was considered analogous to the high-compliance matrix material in the composite, with the unthermoformed material analogous to the low-compliance fiber. Using the isotropic parameters E_m, ν_m, E_f, and ν_f for the elastic moduli of the thermoformed (high-compliance) and unthermoformed (low-compliance) materials, as well as the volume fraction parameters V_m and V_f (related to the relative amounts of high-compliance and low-compliance materials present within the region of interest), a set of orthotropic parameters was calculated using relations adapted from those of Berthelot [10] (summarized in the Appendix). These orthotropic constants are defined for the longitudinal (L, parallel to the strips), transverse (T, perpendicular to the strips), and out-of-plane (T') directions. For each membrane simulated, the equivalent orthotropic parameters for the shear-compliant region were computed using the

relations shown in the Appendix. Although orthotropic materials require more parameters than isotropic materials to fully describe their elastic response, use of this approach allowed the geometrical complexity of the model, and hence the number of elements required, to be significantly reduced. Given that a full-scale solar sail could contain thousands of individual thermoformed strips, it is believed that the use of equivalent orthotropic parameters to model the shear-compliant regions of such membranes will assist in the development of full-scale finite element models of such structures by reducing their geometrical complexity.

IV. Simulation of Wrinkling Under Applied Edge Shear

The wrinkling of membranes under simultaneous edge shear and tension was recently discussed and numerically modeled by Leifer and Belvin [6], Tessler and Sleight [11], and Wong and Pellegrino [12]. Because buckling is a nonlinear process that involves the generation of out-of-plane surface displacements for which the amplitudes are many times larger than the material thickness, a nonlinear *large* displacement analysis was chosen to perform these numerical studies. For all of the finite element models considered here, the nodal degrees of freedom along the transverse edges (parallel to the y direction) of each membrane were clamped. The bottom transverse edge was fixed, whereas a uniform displacement in the longitudinal (x) direction was applied to the top membrane edge (as the first displacement step), thus providing a slight pretension. Small ($\approx$0.001 N) positive and negative out-of-plane "inducement forces" (about six in each of the $\pm z$ directions) were distributed across nodes on the face of each membrane after this pretensioning step, to generate small initial out-of-plane deformations in the model. These forces represent the small imperfections and inhomogeneities present in all physical materials that cause membrane-to-bending coupling in the material. The applied forces were generally chosen to induce out-of-plane surface deformations of no larger than one-half of the membrane thickness. Following this guideline, the particular out-of-plane force distribution chosen had no effect on the final structural wrinkle pattern formed in the pretensioned membrane. After inducing wrinkles in the pretensioned membrane by displacing the top edge of the membrane in the transverse direction in small uniform steps, the out-of-plane inducement forces were released without significantly affecting the shear-induced wrinkle pattern. To minimize the chance of model divergence when releasing the inducement forces, they can be gradually reduced to zero over several load steps using the *Operate/Scale* command in ANSYS and choosing a scale value of less than 1.0 for each step.

Table 1 Model dimensions used for FE simulations of the polyester membrane with a central shear-compliant region

Model dimensions	Value
Width, parallel to direction of strips, m	0.140
Length, perpendicular to direction of strips, m	0.178
Thickness, μm	25.4

Table 2 Number of elements used in each FE model

Model	Number of elements
Model 1 (Fig. 5): detailed 3-D strip shear-compliant region (SHELL 63 elements)	100,000
Model 2 (Fig. 6): flat strip shear-compliant region (SHELL 63 elements)	10,000
Model 3 (Fig. 7): orthotropic approx. shear-compliant region (SHELL 181 elements)	11,954
Model 4 (Fig. 8): no shear-compliant region (SHELL 63 elements)	3905

V. Results

A. Membrane with Central Shear-Compliant Region

Although most effectively deployed along the membrane perimeter, thermoformed shear-compliant regions were first demonstrated by Talley et al. [3] using a test article (shown previously in Fig. 4) that contained a central shear-compliant region. The effect of this shear-compliant region was to ensure that the margins along the top and bottom edges of the membrane remained flat. Two distinct finite element models of this test article were developed in ANSYS using the two simplified approaches for representing the shear-compliant regions outlined earlier. Each approach used about one-tenth the number of elements required for the geometrically realistic FE model reported on previously (Fig. 5) [6]. In addition, a finite element model of an unmodified membrane (not containing a shear-compliant region) was also developed for comparison purposes. The geometrical and material parameters used for each of these models are contained in Tables 1–3.

The results of the finite element simulations are presented in Figs. 6 and 7 and show that each of the modeling approaches undertaken predicted the flat, wrinkle-free top and bottom margins apparent in the photograph of the test object shown on the right side of Fig. 4. The effectiveness of the central shear-compliant zone is further illustrated by the simulation results shown in Fig. 8, which indicates extensive wrinkling throughout a membrane of the same size and material shown previously and which does not contain the central shear-compliant zone. In Figs. 6–8, contour levels represent out-of-plane displacements reported in units of meters and out-of-plane displacements ranging between -0.0029 and $+0.0029$ m were predicted. The shear displacement of the top edge of each model was set at 1.25 mm.

B. Membrane with Shear-Compliant Structures Along its Top and Bottom Edges

To better evaluate the performance of shear-compliant structures as they are intended to function within a solar sail, a 0.2286×0.2286 m square membrane under edge shear was simulated both with and without shear-compliant structures along its top and bottom edges. This particular square geometry was chosen over other possible alternatives because of its prior use in the experimental study of wrinkling as a function of edge shear using photogrammetry (Fig. 9) [13]. In that study, narrow strips of membrane material above

Table 3 Material parameters used in each FE model

Parameter (model 3)	Value	Parameter (model 2)	Value
E_f, E_m, Pa	3.53e9, 0.01e9	E_{nominal}, $E_{\text{thermoformed}}$, Pa	3.53e9, 3.53e6
ν_f, ν_m	0.30, 0.01	ν_{nominal}, $\nu_{\text{thermoformed}}$	0.30, 0.02
K_f, K_m, Pa	3.39e9, 5.03e6		
k_f, k_m, Pa	2.66e9, 1.78e6		
E_L, E_T, $E_{T'}$, Pa	1.77e9, 1.99e7, 1.99e7		
ν_{LT}, $\nu_{TT'}$, $\nu_{LT'}$	0.155, -0.536, $1.75e-6$		
G_{LT}, $G_{TT'}$, $G_{LT'}$, Pa	2.91e7, 2.15e7, 2.15e7		
V_f, V_m	0.5, 0.5		

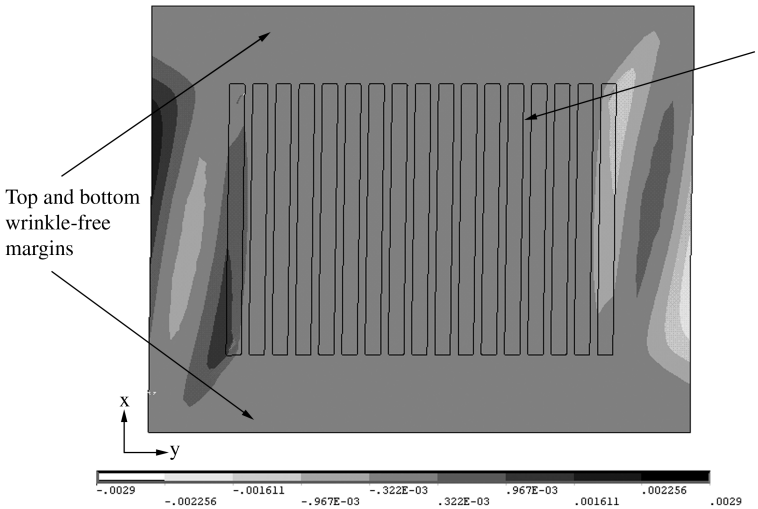

Fig. 6 Finite element model 2, 25-μm-thick membrane with shear-compliant zone modeled using the simplified flat strip geometry. The contours shown represent out-of-plane displacements (m). Transverse and longitudinal displacements of 1.25 mm and 50 μm, respectively, were applied to the clamped top edge of the membrane; the bottom edge was also clamped. Note that the top and bottom margins were predicted to remain flat.

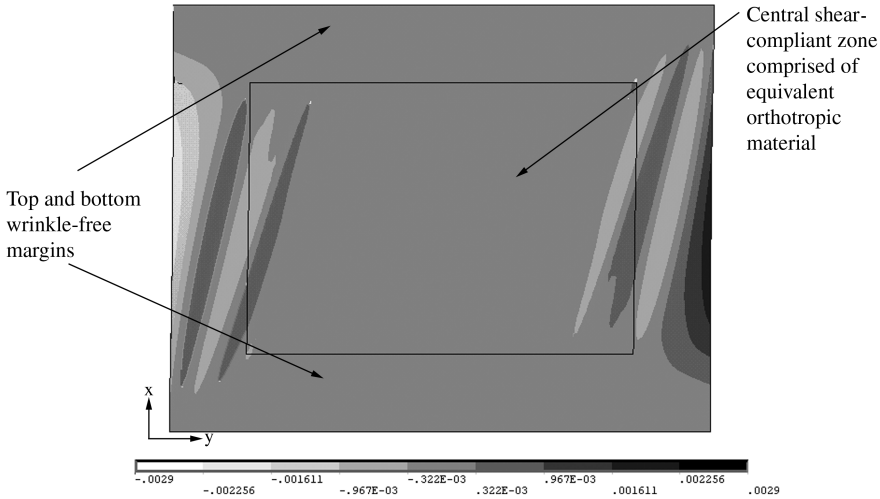

Fig. 7 Finite element model 3, 25-μm-thick membrane with shear-compliant zone modeled using a single orthotropic material. The contours shown represent out-of-plane displacements (m). Transverse and longitudinal displacements of 1.25 mm and 50 μm, respectively, were applied to the clamped top edge of the membrane; the bottom edge was also clamped. Note that the top and bottom margins were predicted to remain flat. The FE model did not converge for transverse edge displacements greater than the 1.25 mm shown in the figure.

and below the top and bottom edges of the square membrane were removed (as an alternative to creating thermoformed strips) to form two shear-compliant regions. This particular approach for forming shear-compliant regions was found (using photogrammetry) to virtually eliminate surface structural wrinkling under a 0.675-mm transverse displacement along the top edge of a 76.2-μm-thick polyester membrane [13].

The finite element models tested used SHELL 181 elements to simulate a 25.4-μm-thick square polyimide membrane and its shear-compliant regions. The aluminum strips shown supporting the top and bottom edges of the test article in Fig. 9 were implemented using eight-node SOLID 45 elements. All boundary displacements were applied uniformly to the nodes on the outer surfaces of the support bars in the finite element model (top surface of the top support and bottom surface of the bottom support). The elements comprising the top and bottom edges of the membrane connected directly to the line of nodes running down the center of the inner surface of each support bar, thus enforcing clamped conditions at these boundaries.

For a membrane similar to the square geometry shown in Fig. 9, wrinkling under an applied edge shear was simulated using both the "alternating high- and low-compliance flat strips" and "uniform orthotropic material" approaches to modeling shear-compliant borders located along the top and bottom edges within the membrane perimeter. Because of the large number of elements required, a model containing a geometrically accurate three-dimensional representation of the shear-compliant strips was not undertaken here. Parameters for all three models tested (two containing each alternative shear-compliant-border formulation, and one without a shear-compliant border) are shown in Tables 4–6.

Figures 10 and 11 show the out-of-plane wrinkling predicted by the finite element code for the polyimide membrane with shear-compliant regions modeled, respectively, using the alternating flat strip and the orthotropic approximation methods. Both models were subjected to the same edge displacements (bottom edge clamped and top edge uniformly displaced 127 μm vertically and 381 μm horizontally). As with the prior series of results predicted (Figs. 6–8), the contours represent out-of-plane membrane displacement, with units expressed in meters, and similar amounts of wrinkling were predicted for both membranes containing the shear-compliant borders. Although these shear-compliant borders have clearly not been optimized, they reduce both the amplitude and extent of wrinkling predicted for a membrane of the same overall dimensions that does not contain shear-compliant features (Fig. 12).

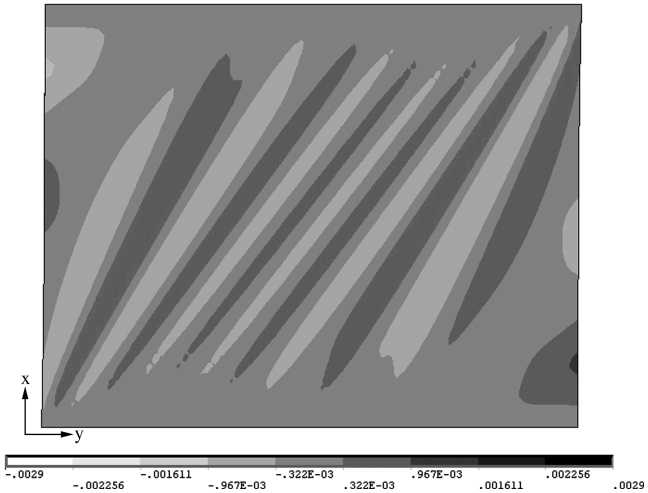

Fig. 8 Finite element model 4, 25-μm-thick membrane with no shear-compliant structures (for comparison). The contours shown represent out-of-plane displacements (m). Transverse and longitudinal displacements of 1.25 mm and 50 μm, respectively, were applied to the clamped top edge of the membrane; the bottom edge was also clamped. Note that shear-induced wrinkling is present throughout the entire extent of the membrane.

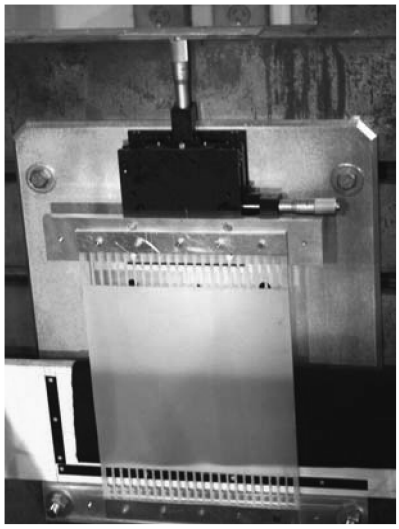

Fig. 9 Two 0.0381-m-long shear-compliant borders on the horizontal edges of a 0.2286 × 0.2286 m membrane. Material shown is 76.2-μm-thick polyester. Shear and tension in the membrane were controlled via positioning micrometers shown supporting the top of the membrane (from Leifer et al. [13]).

VI. Discussion

The simulations presented here simply demonstrate two approaches for representing the complex geometric structure of a shear-compliant border: one that contains alternating strips of high-compliant and low-compliant materials and a second that models the shear-compliant region with one single orthotropic material. Using the data shown in Tables 1–6, both approaches provided quantitatively similar results for the two different geometries and membrane materials tested. For the polyester-membrane models containing the central shear-compliant region (Figs. 6 and 7), near-identical nonwrinkled regions were predicted within the upper and lower margins of the membranes under simultaneous 50-μm longitudinal and 1.25-mm transverse edge displacements. These numerical results mimic the flat, wrinkle-free regions apparent within the photograph of the test article shown on the right side of Fig. 4. For the square-polyimide-membrane models containing the shear-compliant regions at their top and bottom edges, both the amplitude and extent of the predicted wrinkle patterns within the central region are much smaller (Figs. 10 and 11) than those predicted for an unmodified membrane (Fig. 12) under a simultaneous 127-μm longitudinal and −381-μm transverse edge displacement.

One question that arose during the course of the research pertained to how the material parameters used to simulate the shear-compliant regions were chosen. Although the high values of Young's modulus (E_{high}) chosen for each of the models simulated were based on previously published data, the low values of Young's modulus (E_{low}) used to implement the shear-compliant regions were initially chosen based on the experiments of Greschik and Mikulas [7] discussed previously. To test the sensitivity of each modeling approach to the ratio of $E_{\text{high}}/E_{\text{low}}$, a parameter study was performed using the square-polyimide-membrane models containing the shear-compliant regions at their top and bottom edges. This particular geometry was chosen for the parameter study because the location of the shear-compliant regions along the membrane's top and bottom edges most closely resembles that proposed for the integrated shear-compliant borders to be used in the planned full-sized and scale-model prototypes depicted in Figs. 1 and 2. Tables 7 and 8 contains the $E_{\text{high}}/E_{\text{low}}$ ratios used in the parameter study. Figure 13 shows the

Table 4 Model dimensions used for FE simulation of the square polyimide membrane with shear-compliant zones along its top and bottom edges

Dimensions	Value
Width, parallel to direction of strips, m	0.2286
Length, perpendicular to direction of strips, m	0.2286
Thickness, μm	25.4

Table 5 Number of elements used in each FE model

Model	Number of elements
Model 5 (Fig. 10): flat strip shear-compliant region (SHELL 181 elements)	17,905
Model 6 (Fig. 11): orthotropic approx. shear-compliant region (SHELL 181 elements)	14,375
Model 7 (Fig. 12): no shear-compliant region (SHELL 181 elements)	14,145

Table 6 Model dimensions used for FE simulation of the square polyimide membrane with shear-compliant zones along its top and bottom edges

Parameter (model 6)	Value	Parameter (model 5)	Value
E_f, E_m, Pa	2.95e9; 0.0095e9	E_{nominal}, $E_{\text{thermoformed}}$, Pa	2.59e9, 2.59e6
ν_f, ν_m	0.34, 0.01	ν_{nominal}, $\nu_{\text{thermoformed}}$	0.34, 0.02
K_f, K_m, Pa	3.34e9, 4.80e6		
k_f, k_m, Pa	2.86e9, 1.69e6		
E_L, E_T, $E_{T'}$, Pa	1.48e9, 1.89e7, 1.89e7		
ν_{LT}, $\nu_{TT'}$, $\nu_{LT'}$	0.175, −0.536, 2.24e − 3		
G_{LT}, $G_{TT'}$, $G_{LT'}$, Pa	2.76e7, 2.04e7, 2.04e7		
V_f, V_m	0.5, 0.5		

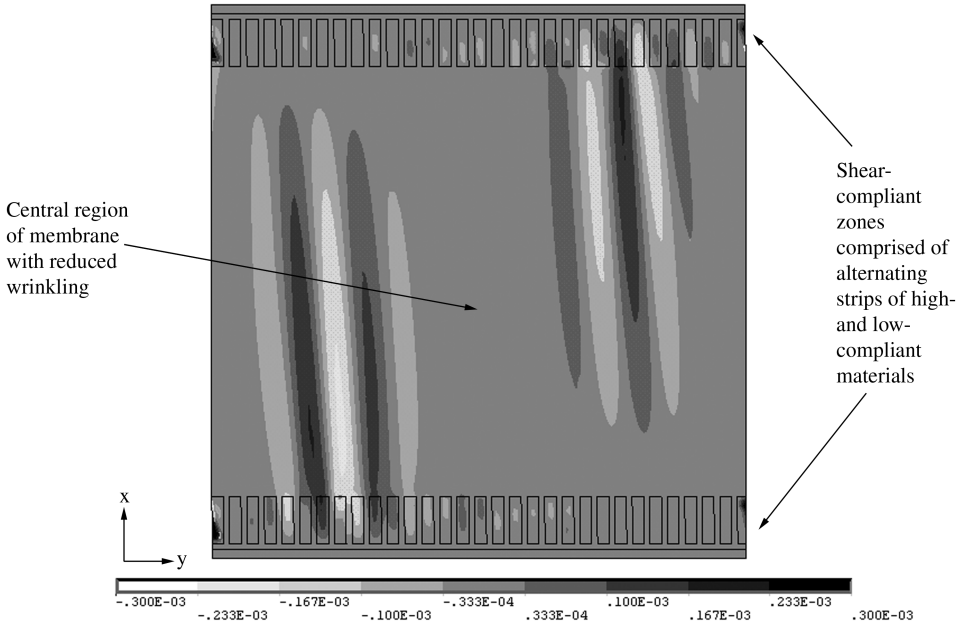

Fig. 10 Finite element model 5, 25.4-μm-thick polyimide membrane containing shear-compliant zones modeled using simplified low- and high-compliance flat strips along its top and bottom edge. The contours shown represent out-of-plane displacements (m). Transverse and longitudinal displacements of −381 and 127 μm, respectively, were applied to the clamped top edge of the membrane; the bottom edge was also clamped.

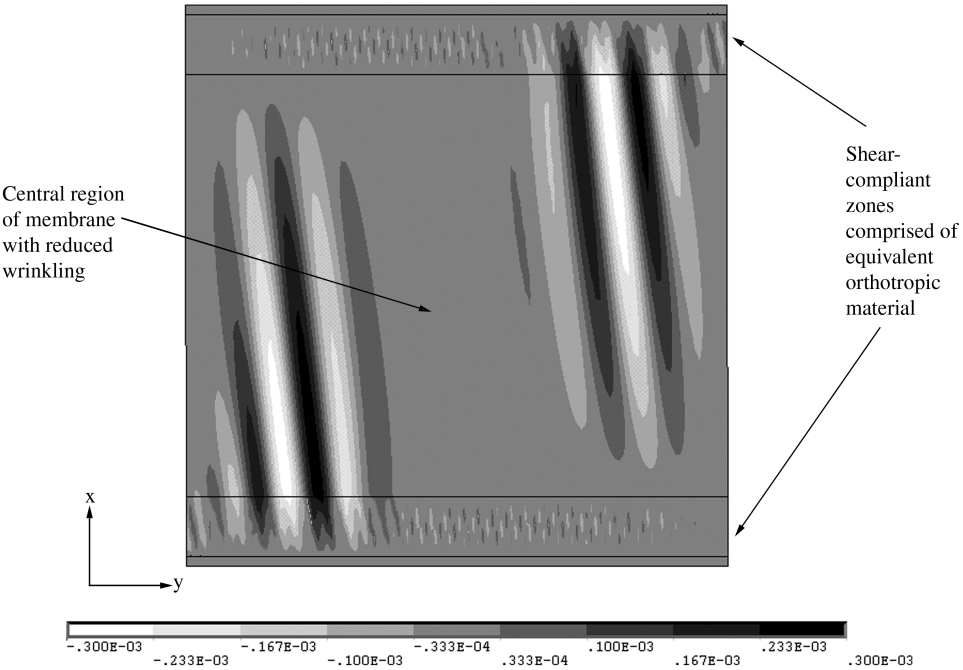

Fig. 11 Finite element model 6, 25.4-μm-thick polyimide membrane containing shear-compliant zones modeled using single orthotropic regions along its top and bottom edges. The contours shown represent out-of-plane displacements (m). Transverse and longitudinal displacements of −381 and 127 μm, respectively, were applied to the clamped top edge of the membrane; the bottom edge was also clamped.

results obtained by varying the $E_{\text{nominal}}/E_{\text{thermoformed}}$ ratio from 10^4 to 10^2 for the model containing alternating high- and low-compliance flat strips along its upper and lower edges. Similarly, Fig. 14 contains the results obtained by varying the E_f/E_m ratio from 10^3 to 10^2 for the model that used a single orthotropic area to depict each shear-compliant border. Both figures use the same contour scales to depict out-of-plane displacements in meters, and all simulations were subjected to the same transverse and longitudinal displacement inputs along the top edge. The results of this study show that for the particular geometry and edge displacements simulated, the model composed of simplified flat strips of alternating low- and high-stiffness materials, depicted in Fig. 13, is much less sensitive to changes in the $E_{\text{nominal}}/E_{\text{thermoformed}}$ ratio than the model that used a single orthotropic material to represent each shear-compliant border, shown in Fig. 14.

The results shown in this paper were obtained primarily to demonstrate the potential effectiveness of using simplified approaches in place of modeling the full three-dimensional details of thermoformed shear-compliant regions. For this reason, no attempt was made to optimize the performance of the shear-compliant borders evaluated here by varying their respective geometries within the particular membranes simulated. Although using either simplified scheme for modeling shear-compliant regions of square membranes under edge shear clearly shows promise, a

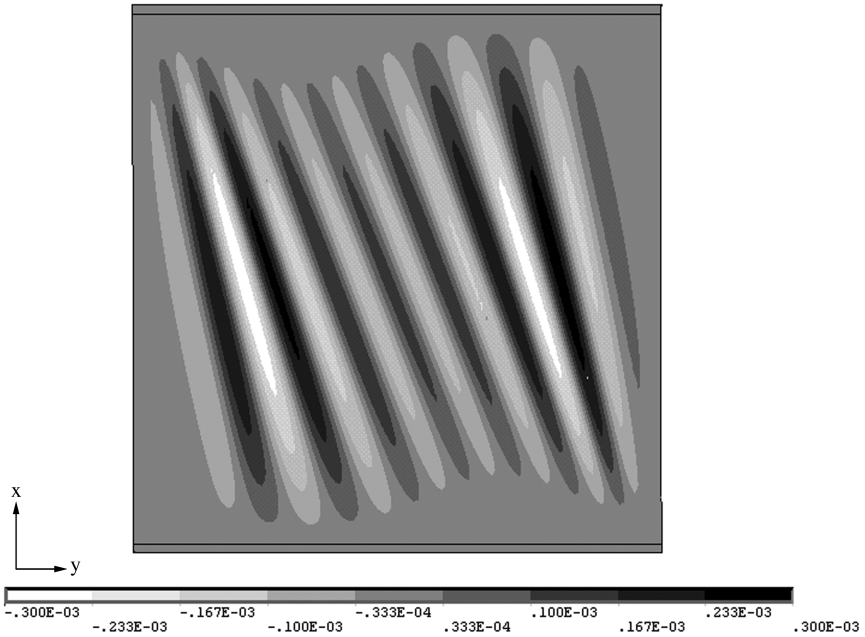

Fig. 12 Finite element model 7, 25.4-μm-thick polyimide membrane without shear-compliant zones. The contours shown represent out-of-plane displacements (m). Transverse and longitudinal displacements of −381 and 127 μm, respectively, were applied to the clamped top edge of the membrane; the bottom edge was also clamped.

similar study of developing techniques to reduce the complexity of models for shear-compliant regions in triangular membrane panels, such as those shown in Figs. 1–3, must be undertaken as the next step in verifying this approach for modeling the behavior of full-size shear-compliant solar sails. Furthermore, full confidence in the effectiveness of the modeling technique can only be obtained by quantitatively comparing the numerical results obtained for models using these approaches with experimental measurements of corresponding scale-model prototypes containing shear-compliant regions.

VII. Conclusions

Two possible strategies for incorporating shear-compliant regions into finite element models of membranes were demonstrated. Although the method that uses alternating thin, flat strips of low-compliance/high Poisson's ratio and high-compliance/near-zero Poisson's ratio elements is straightforward and represents a dramatic reduction in complexity over that of the full three-dimensional representation, each strip must be individually added to the finite element model. Therefore, this approach may be too complex for full-scale solar sail models containing thousands of thermoformed strips along the membrane edges. In contrast, although the results of implementing the shear-compliant regions using one single uniaxial orthotropic material region along each clamped membrane edge will result in a geometrically simpler model, the parameter study indicates that results may be quite sensitive to the choice of material parameters. For the limited number of cases simulated here, both approaches for simulating shear-compliant regions within a membrane could be designed to yield quantitatively similar results. However, a more systematic and exhaustive study (including incorporating a membrane shape more representative of that envisioned for use in a full-scale solar sail and supplemented, if possible, by experimental measurement on scale models) must all be completed before final conclusions about this approach are drawn.

Table 7 Values of Young's modulus used for the simplified strip implementation (model 5; Fig. 13) parameter study

Case number	E_{high} (E_{nominal}), Pa	E_{low} ($E_{\text{thermoformed}}$), Pa	Ratio ($E_{\text{high}}/E_{\text{low}}$)
5A	2.95e9	2.95e5	10,000
5B	2.95e9	2.95e6	1000
5C	2.95e9	2.95e7	100

Table 8 Value of Young's Modulus used for the orthotropic region implementation (model 6; Fig. 14) parameter study

Case number	E_{high} (E_f), Pa	E_{low} (E_m), Pa	Ratio ($E_{\text{high}}/E_{\text{low}}$)
6A	2.95e9	2.95e6	1000
6B	2.95e9	5.00e6	590
6C	2.95e9	9.50e6	311
6D	2.95e9	2.95e7	100

Appendix: Calculation of Orthotropic Parameters

The behavior of a unidirectional orthotropic material is fully defined by specifying the values of five independent moduli such as $E_L, E_T, \nu_{LT}, G_{LT}$, and $G_{TT'}$. The values of these five constants can be calculated using only the isotropic material parameters E_m and ν_m for the Young's modulus and Poisson ratio of the thermoformed strips, E_f and ν_f for the corresponding parameters of the bulk membrane material, and volume fraction parameters V_m and V_f related to the relative amounts of low- and high-compliance material that comprise the shear-compliant region. According to Berthelot [10], a number of different approaches (e.g., the law of mixtures and Halpin–Tsai relations) can be used to calculate the equivalent orthotropic moduli from the isotropic parameters and different methods yield slightly different results. For the dependent isotropic parameters used here (calculated from the values of E and ν of the membrane material and the values used to approximate E and ν for the thermoformed strips),

$$G_i = \frac{E_i}{1 + 2\nu_i} \tag{A1}$$

$$K_i = \frac{E_i}{2(1 - 2\nu_i)(1 + \nu_i)} \tag{A2}$$

and

$$k_i = K_i - \frac{G_i}{3} \tag{A3}$$

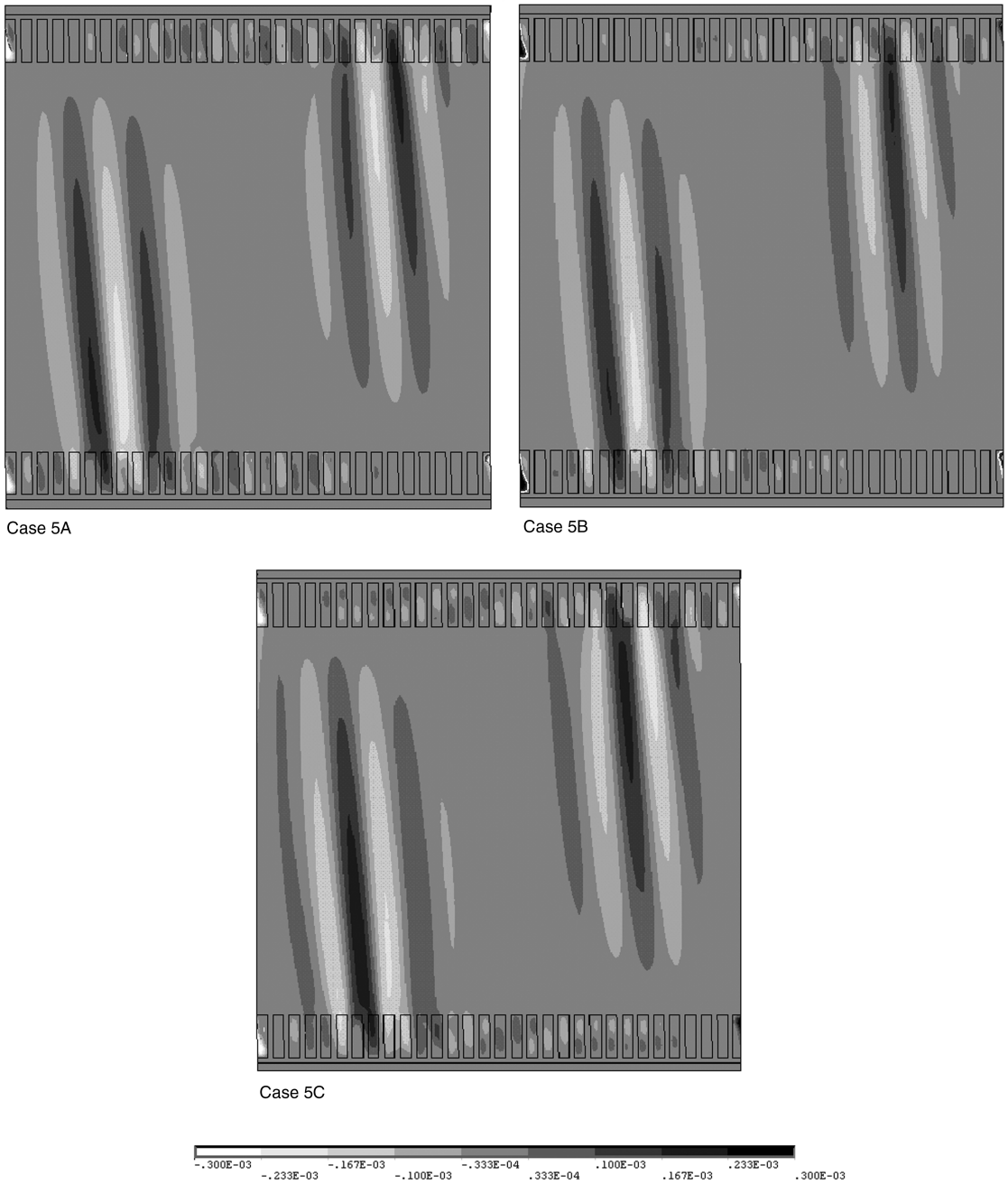

Fig. 13 Effect of changing E_{low} ($E_{\text{thermoformed}}$) in 25.4-μm-thick polyimide-membrane model under simulated top-edge transverse and longitudinal displacements of −381 and 127 μm. Simulation results for shear-compliant zone implemented using alternating high- and low-compliance strips demonstrate that model performance is essentially independent of stiffness ratios ($E_{\text{high}}/E_{\text{low}}$) of 10,000, 1000 and 100, shown, respectively, by cases 5A, 5B, and 5C.

where the parameters for the low- and high-compliance materials are obtained by substituting m and f for i, respectively. Using the dependent and independent isotropic parameters calculated earlier, the orthotropic parameters can then be estimated using

$$E_L = E_f V_f + E_m V_m \tag{A4}$$

$$E_T = \frac{E_m}{1 + [(E_m/E_f) - 1]V_f} \tag{A5}$$

$$\nu_{LT} = \nu_f V_f + \nu_m V_m \tag{A6}$$

$$\nu_{TL} = \nu_{LT}\left(\frac{E_T}{E_L}\right) \tag{A7}$$

$$G_{LT} = G_m\left[\frac{G_f(1 + V_f) + G_m V_m}{G_f V_m + G_m(1 + V_f)}\right] \tag{A8}$$

$$G_{TT'} = G_m\left[1 + V_f\left(\frac{G_m}{G_f - G_m} + \frac{V_m(k_m + \frac{7}{3}G_m)}{2k_m + \frac{8}{3}G_m}\right)^{-1}\right] \tag{A9}$$

and

$$\nu_{TT'} = \frac{E_T}{2G_{TT'}} - 1 \tag{A10}$$

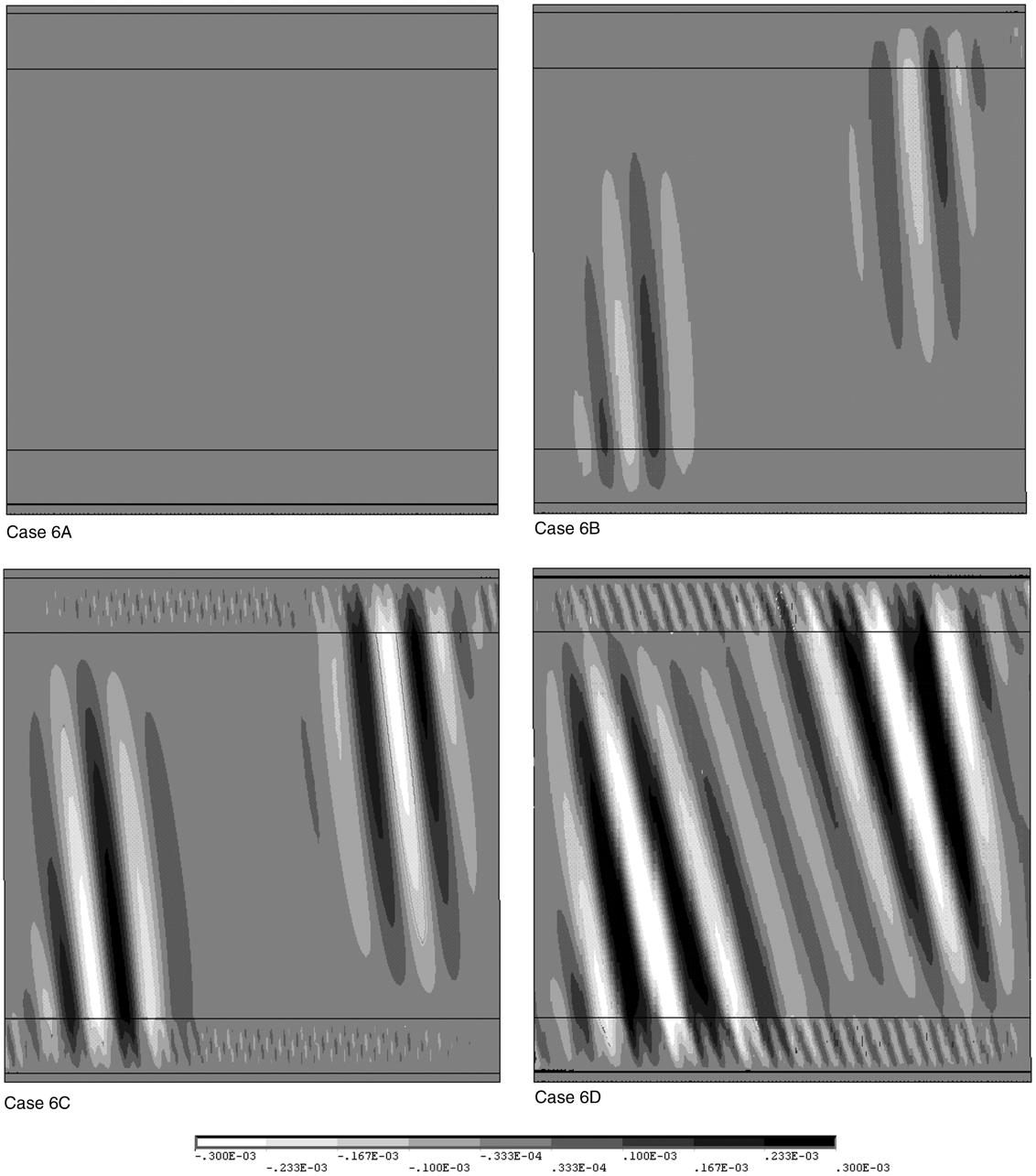

Fig. 14 Effect of changing E_{low} (E_m) in 25.4-μm-thick polyimide-membrane model under simulated top-edge transverse and longitudinal displacements of −381 and 127 μm. Simulation results for shear-compliant zone implemented using an equivalent orthotropic material demonstrate that model performance varies substantially as a function of stiffness ratios (E_{high}/E_{low}) of 1000, 590, 311, and 100 shown, respectively, by cases 6A, 6B, 6C, and 6D.

subject to

$$V_m + V_f = 1 \tag{A11}$$

The relations shown in Eqs. (A4–A11) were compiled and adapted using material from Berthelot [10].

Acknowledgments

The author completed part of the work for this paper while participating in the NASA Faculty Fellowship Program at the NASA Langley Research Center and completed the computational simulations using resources provided by both the University of Kentucky and Trinity University. Additional support for this work was provided by the Tom and Mary Turner Junior Faculty Fellowship for Summer Research at Trinity University. He is grateful for the insights of W. Keith Belvin of the NASA Langley Research Center, who initially suggested modeling the shear-compliant region as a single orthotropic material.

References

[1] Lichodziejewski, D., Derbès, B., West, J., Reinert, R., Belvin, W. K., and Pappa, R. "Bringing an Effective Solar Sail Design Toward TRL 6," 39th AIAA/ASME/SAE/ASEE Joint Propulsion Conference, Huntsville, AL, AIAA Paper 2003-4659, 2003.

[2] Adler, A. L., Mikulas, M. M., and Hedgepeth, J. M., "Static and Dynamic Analysis of Partially Wrinkled Membrane Structures," 41st AIAA/ASME/ASCE/AHS/ASC Structures, Structural Dynamics and Materials Conference, Atlanta, GA, AIAA Paper 2000-1810, Apr. 2000.

[3] Talley, C., Clayton, W., Gierow, P., McGee, J., and Moore, J., "Advanced Membrane Materials for Improved Solar Sail Capabilities," 43rd AIAA/ASME/ASCE/AHS/ASC Structures, Structural Dynamics and Materials Conference, Denver, CO, AIAA Paper 2002-1561, Apr. 2002.

[4] Murphy, D., Trautt, T., McEachen, M., Eskenazi, M., Messner, D., Laue, G., and Gierow, P., "Progress and Plans for System Demonstration of a Scalable Square Solar Sail," 14th AAS/AIAA Space Flight Mechanics Conference, Maui, HA, American Astronautical Society Paper AAS 04-105, Feb. 2004.

[5] Murphey, T. W., Murphy, D., Mikulas, M. M., Jr., Adler, A. L., "A Method to Quantify the Thrust Degradation Effects of Structural Wrinkles in Solar Sails," 43rd AIAA/ASME/ASCE/AHS/ASC Structures, Structural Dynamics and Materials Conference, Denver, CO, AIAA Paper 2002-1560, Apr. 2002.

[6] Leifer, J., and Belvin, W. K., "Prediction of Wrinkle Amplitudes in Thin Film Membranes Using Finite Element Modeling," 44th AIAA/ASME/ASCE/AHS/ASC Structures, Structural Dynamics and Materials Conference, Norfolk, VA, AIAA Paper 2003-1983, Apr. 2003.

[7] Greschik, G., and Mikulas, M. M., "On Imperfections and Stowage Creases in Aluminum Rigidized Inflated Cylinders," 37th AIAA/ASME/ASCE/AHS/ASC Structures, Structural Dynamics and Materials Conference, Salt Lake City, UT, AIAA Paper 1996-1332, Apr. 1996.

[8] Murphey, T. W., "The Constitutive Modeling of Thin Films with Random Material Wrinkles," 42nd AIAA/ASME/ASCE/AHS/ASC Structures, Structural Dynamics and Materials Conference and Exhibit, Seattle, WA, AIAA Paper 2001-1347, Apr. 2001.

[9] Murphey, T. W., "A Nonlinear Elastic Constitutive Model for Wrinkled Thin Films," Ph.D. Thesis, Department of Mechanical Engineering, Univ. of Colorado at Boulder, Boulder, CO, 2000.

[10] Berthelot, J-M., "Elastic Behavior of Unidirectional Composite Materials," *Composite Materials*, Springer–Verlag, New York, 1999, Chap. 9.

[11] Tessler, A., and Sleight, D., "Toward Effective Shell Modeling of Wrinkled Thin-Film Membranes Exhibiting Stress Concentrations," 45th AIAA/ASME/ASCE/AHS/ASC Structures, Structural Dynamics and Materials Conference, Palm Springs, CA, AIAA Paper 2004-1739, 2004.

[12] Wong, Y. W., and Pellegrino, S., "Computation of Wrinkle Amplitudes in Thin Membranes," 43rd AIAA/ASME/ASCE/AHS/ASC Structures, Structural Dynamics and Materials Conference, Denver, CO, AIAA Paper 2002-1369, 2002.

[13] Leifer, J., Black, J. T., Belvin, W. K., and Behan, V., "Design and Evaluation of Shear-Compliant Borders for Thin Film Membrane Structures," 44th AIAA/ASME/ASCE/AHS/ASC Conference on Structures, Structural Dynamics and Materials, Norfolk, VA, AIAA Paper 2003-1984, 2003.

[14] Gaspar, J. L., Mann, T., Behun, V., Keats Wilkie, W., and Pappa, R., "Development of Modal Test Techniques for Validation of a Solar Sail Design," 45th AIAA/ASME/ASCE/AHS/ASC Structures, Structural Dynamics and Materials Conference: Gossamer Structures Forum, Palm Springs, CA, AIAA Paper 2004-1665, Apr. 2004.

D. Edwards
Associate Editor